bioRxiv preprint doi: https://doi.org/10.1101/2023.03.28.534566; this version posted March 29, 2023. The copyright holder for this preprint (which was not certified by peer review) is the author/funder, who has granted bioRxiv a license to display the preprint in perpetuity. It is made available under aCC-BY 4.0 International license.

Micro to macro scale analysis of the intact human renal arterial tree with Synchrotron Tomography

Rahmani, Shahrokh[1]; Jafree, Daniyal J.[2,3]; Lee, Peter D.[1]; Tafforeau, Paul[4]; Jacob, Joseph[5,6]; Bellier, Alexandre[7];Ackermann, Maximilian[8,9]; Jonigk, Danny D. [10,11]; Shipley, Rebecca J.[1]; Long, David A.[2]; Walsh, Claire L.[1]

[1]*Department of Mechanical Engineering, University College London, London, UK, WC1E 6BT*

[2]*Developmental Biology and Cancer Research & Teaching Department, UCL Great Ormond Street Institute of Child Health, University College London, London, UK, WC1N 1EH*

[3] *UCL MB/PhD Programme, Faculty of Medical Science, University College London, London, UK, WC1E 6BT*

[4]*European Synchrotron Radiation Facility, Grenoble, France, 38043*

[5]*Satsuma Lab, Centre for Medical Image Computing, UCL, London, UK*

[6]*Lungs for Living Research Centre, UCL, London, UK*

[7]*Department of Anatomy (LADAF), Grenoble Alpes University, Grenoble, France, 38058*

[8]*Institute of Anatomy, University Medical Center of the Johannes Gutenberg University Mainz, Mainz, Germany*

[9]*Institute of Pathology and Department of Molecular Pathology, Helios University Clinic Wuppertal, University of Witten-Herdecke, Wuppertal, Germany*

[10]*Institute of Pathology, RWTH Aachen Medical University, Aachen, Germany*

[11]*German Center for Lung Research (DZL), Biomedical Research in Endstage and Obstructive Lung Disease Hannover (BREATH), Hannover, Germany*

Correspondence: Dr Shahrokh Rahmani, Dr Claire L. Walsh and Professor Peter D. Lee,

Mechanical Engineering, University College London, London, UK, WC1E 6BT

Email: s.rahmani@ucl.ac.uk; c.walsh.11@ucl.ac.uk; peter.lee@ucl.ac.uk

bioRxiv preprint doi: https://doi.org/10.1101/2023.03.28.534566; this version posted March 29, 2023. The copyright holder for this preprint (which was not certified by peer review) is the author/funder, who has granted bioRxiv a license to display the preprint in perpetuity. It is made available under aCC-BY 4.0 International license.

SIGNIFICANCE STATEMENT

High-resolution, three-dimensional, renal vasculature models are currently highly reliant on data obtained from rodent kidneys. Obtaining this information in a human kidney is difficult, given its size and scale. Here, we overcome this challenge through synchrotron-based imaging to profile the vasculature of an intact human kidney. Organ-wide vascular network metrics are shown to be largely conserved between human and rat kidneys. Regional and spatial heterogeneities between cortical, medullary, and hilar vascular architecture are revealed, highlighting a structural basis for renal oxygen gradients in humans. This is, to our knowledge, the first time the vasculature of a human kidney has been mapped in its entirety, with implications for understanding how the hierarchy of individual blood vessel segments collectively scales to renal function.

bioRxiv preprint doi: https://doi.org/10.1101/2023.03.28.534566; this version posted March 29, 2023. The copyright holder for this preprint (which was not certified by peer review) is the author/funder, who has granted bioRxiv a license to display the preprint in perpetuity. It is made available under aCC-BY 4.0 International license.

ABSTRACT

Background: The kidney vasculature is exquisitely structured to orchestrate renal function. Structural profiling of the vasculature in intact rodent kidneys, has provided insights into renal haemodynamics and oxygenation, but has never been extended to the human kidney beyond a few vascular generations. We hypothesised that synchrotron-based imaging of a human kidney would enable assessment of vasculature across the whole organ.

Methods: An intact kidney from a 63-year-old male was scanned using hierarchical phase-contrast tomography (HiP-CT), followed by semi-automated vessel segmentation and quantitative analysis. These data were compared to published micro-CT data of whole rat kidney.

Results: The intact human kidney vascular network was imaged with HiP-CT at 25 μm voxels, representing a 20-fold increase in resolution compared to clinical CT scanners. Our comparative quantitative analysis revealed the number of vessel generations, vascular asymmetry and a structural organisation optimised for minimal resistance to flow, are conserved between species, whereas the normalised radii are not. We further demonstrate regional heterogeneity in vessel geometry between renal cortex, medulla, and hilum, showing how the distance between vessels provides a structural basis for renal oxygenation and hypoxia.

Conclusions: Through the application of HiP-CT, we have provided the first quantification of the human renal arterial network, with a resolution comparable to that of light microscopy yet at a scale several orders of magnitude larger than that of a renal punch biopsy. Our findings bridge anatomical scales, profiling blood vessels across the intact human kidney, with implications for renal physiology, biophysical modelling, and tissue engineering.

bioRxiv preprint doi: https://doi.org/10.1101/2023.03.28.534566; this version posted March 29, 2023. The copyright holder for this preprint (which was not certified by peer review) is the author/funder, who has granted bioRxiv a license to display the preprint in perpetuity. It is made available under aCC-BY 4.0 International license.

INTRODUCTION

The kidney receives up to 20% of cardiac output, carried into the organ by arteries branching off the abdominal aorta and entering the renal hilum. Once within the kidney, the renal arteries divide hierarchically, into interlobar and interlobular vessels enroute to the renal cortex and, within the cortex, as arcuate arteries and efferent arterioles. This network perfuses specialised glomerular capillaries for plasma ultrafiltration, before peritubular capillaries and vasa recta facilitate dynamic solute exchange. Thereafter, venous return follows the arterial supply out of the organ.[1]

Structural and molecular changes to the renal vasculature accompanied by alterations in tissue oxygenation occur in diabetes, hypertension, transplant rejection and chronic kidney disease in both animal models and patients.[2] Studying renal vascular structure and heterogeneities thus has implications for understanding the basis of renal function in health and disease. Advances in imaging modalities such as micro-computed tomography (μCT),[3–5] magnetic resonance imaging (MRI)[6], lightsheet microscopy (LSM)[8,9,] and photoacoustic imaging[10] have generated detailed analyses of blood vessels in intact mammalian kidneys, particularly rodents.[5] Although LSM has been used to quantify cortical vessel diameters in humans,[11] it has not captured the intact renal vascular network of the human kidney without tissue subsampling.

Here, we map the intact arterial network of an entire human kidney using Hierarchical Phase-contrast Tomography (HiP-CT).[12] Previously, we quantified glomerular morphology across cubic centimetres of intact human kidney with HiP-CT[12] and now we extend HiP-CT analysis to the topology of the intact human renal arterial network. We compare topological metrics between rodent and human kidneys and identify spatial heterogeneities that may contribute to oxygenation gradients within the intact human organ.

bioRxiv preprint doi: https://doi.org/10.1101/2023.03.28.534566; this version posted March 29, 2023. The copyright holder for this preprint (which was not certified by peer review) is the author/funder, who has granted bioRxiv a license to display the preprint in perpetuity. It is made available under aCC-BY 4.0 International license.

METHODS

Sample preparation

An intact human right kidney was obtained from a 63-year-old male (cause of death: pancreatic cancer) who consented to body donation to the Laboratoire d'Anatomie des Alpes Françaises, (Grenoble, France) before death. Post-mortem study was conducted according to Quality Appraisal for Cadaveric Studies scale recommendations.[13] The body was embalmed by injecting 4500 mL of 1.15% formalin in lanolin followed by 1.44% formalin into the right carotid artery, before storage at 3.6 °C. During evisceration of the kidney, vessels were exposed, and surrounding fat and connective tissue removed. The kidney was post-fixed in 4% neutral-buffered formaldehyde at room temperature for one week. The kidney was then dehydrated through an ethanol gradient over 9 days to a final equilibrium of 70%.[14] The volume of each dehydration solution was four-fold greater than the volume of the organ and during dehydration, the solution was degassed using a diaphragm vacuum pump (Vacuubrand, MV2, 1.9m3/h) to remove excess dissolved gas. The dehydrated kidney was transferred to a polyethylene terephthalate jar where it was physically stabilised using a crushed agar-agar ethanol mixture, and then imaged.[12,14]

Scanning, image acquisition and reconstruction

Imaging was performed on the BM05 beamline at the ESRF following the HiP-CT protocol.[12,14] Initially the whole kidney was imaged at 25 µm/voxel (edge length). Volumes of interest within the same kidney were also imaged at 6.5 and 2.6 µm/voxel.[12] Tomographic reconstruction was performed[12,14] using PyHST2 software[15]. Briefly, a filtered back-projection algorithm with single-distance phase retrieval coupled to an unsharp mask filter was applied to the collected radiographs. The reconstructed volumes at all three scales were binned (average binning) to 50, 13, and 5.2 μm^3/voxel, respectively, to reduce computational load

bioRxiv preprint doi: https://doi.org/10.1101/2023.03.28.534566; this version posted March 29, 2023. The copyright holder for this preprint (which was not certified by peer review) is the author/funder, who has granted bioRxiv a license to display the preprint in perpetuity. It is made available under aCC-BY 4.0 International license.

for subsequent image segmentation and quantification. (Scanning parameters can be found in Supplementary **Table S1**)

Image filtering, enhancement, and segmentation

Prior to semi-automated segmentation, images were filtered to enhance blood vessel wall contrast. A 3D median filter (iterative and 26-adjacent analysis) was used to reduce image noise; image normalisation was performed using background detection correction (Amira v2021.1; type: B-spline, voxel dimensions: 91, 130, 227). Semi-automated segmentation of the arterial networks was performed in Amira v2021.1 using a region growing tool. In this method, the user selects seed locations and an intensity threshold, then any pixels within the connected neighbourhood of the seed point and within the threshold are added to the region, and this continues in an iterative fashion expanding the region. The annotator continues to select seed points and thresholds until the interior of all vessels are filled. This method was applied to segment the whole renal arterial network from the intact human kidney from the imaging data at 50 μm^3/voxel, and portions of the same network in the 13 and 5.2 μm^3/voxel datasets. The segmentations were proof read by a second independent annotator and segmentation between the initial and the second annotator were iterated until no further changes were found. Arteries and veins, were distinguished due to the thicker walls of arteries, and ultimate connectivity to the renal artery.

Visualization and skeletonization

To quantify the human kidney blood vasculature, the segmented 3D vascular network at 50 μm^3/voxel was skeletonized using the centreline tree algorithm in Amira (tube parameters: slope = 6 and zeroval = 16). The resulting spatial graph describes the vascular network in terms of ‘points’, ‘segments’, and ‘vessels’ with definitions for each shown in **Fig.S1A**. A vessel was defined as the connector between a start and end point, which corresponds to either a branching point leading into another vessel branch or a terminal end where no

bioRxiv preprint doi: https://doi.org/10.1101/2023.03.28.534566; this version posted March 29, 2023. The copyright holder for this preprint (which was not certified by peer review) is the author/funder, who has granted bioRxiv a license to display the preprint in perpetuity. It is made available under aCC-BY 4.0 International license.

further branches were detectable. Segments are assumed to be cylinders with a circular cross section joining points that discretise the vessel length.

Morphological analysis

To assess vessel generations, two methods were applied, i) a 'topological' approach, starting from the renal artery as generation one, with each branching point increasing the generation number by one **(Fig.1D)**; ii) the Strahler ordering system, where the terminal ends of the network are assigned as the first order apart from a single manually selected point which is designated as the root point (the renal artery in this case), iterating through the network from these end points, at every branch points, when two vessels with the same order intersect, the resulting vessel has an order one greater. Alternatively, if two vessels with different orders intersect, the higher generation of the two is given to the resulting vessel **(Fig.1E)**. Morphological metrics of the network were calculated from the spatial graph as follows (see also **Figure S1A)**:

1) Branching angle: the angle between the two daughter vessels from a common parent vessel, where the vessel vectors are considered to be the Euclidean path between the common branching point of the parent and the two daughters and the end points for each daughter vessel
2) Tortuosity: the Euclidean distance between the start and end points of a vessel divided by the sum of all lengths of segments that make up that vessel,
3) Radius: calculated for each vessel as the mean of all segment radii, or in the case of vessel partial collapse, the maximum segment radius or in the case of complete vessel collapse, an equivalent radius for the perimeter of vessel cross-section in the binary image.
4) Length: the sum of all distances between points in a single vessel
5) Branching ratio: the number of vessels of a given generation/order divided by the number vessels of the order or generation above.

bioRxiv preprint doi: https://doi.org/10.1101/2023.03.28.534566; this version posted March 29, 2023. The copyright holder for this preprint (which was not certified by peer review) is the author/funder, who has granted bioRxiv a license to display the preprint in perpetuity. It is made available under aCC-BY 4.0 International license.

6) Adherence to Murray's Law: this states that the cube of the parent vessel diameter should be equal to the sum of the cubed daughter vessel diameters, and was assessed by analysing the measurements of vessel diameters and branching points. Murray's Law suggests that the blood flow in a network is distributed in a manner that minimizes resistance to flow when the diameters of the parent and daughter vessels are in a certain ratio.
7) Inter-vessel distance, used to infer tissue perfusion and oxygenation across the human kidney due to its correlation with diffusion distance, was calculated as the distance of every tissue voxel from its nearest vessel voxel *via* a 3D distance transform applied to the binary vessel image. All codes for the calculation of the above metrics are provided in Supplementary Data.

These metrics can provide insights into the mechanisms underlying the formation and maintenance of the vascular network, as well as the functional implications of deviations from Murray's Law. Additionally, the above metrics in our human kidney were compared to those of the rat kidney taken from Nordsletten et al.[5] scanned at 20 μm^3/voxel using a micro CT scanner, where a radiopaque silicone polymer was perfused to enhance contrast.[5]

Kidney Compartment Segmentation

Segmentation of the compartments within the human kidney, including cortex, medulla and hilum, was performed in Dragonfly (version: 2021.3) using the segmentation wizard to train a 2D convolutional neural network (CNN). The final hyperparameters of the CNN are given in **Table S2**. Manual correction of the CNN output was performed in Amira (v2021.1), to provide the final compartment segmentation. These segmentations were used to compare the inter-vessel distance variation between the cortex, medulla, and hilum.

Statistical analysis

bioRxiv preprint doi: https://doi.org/10.1101/2023.03.28.534566; this version posted March 29, 2023. The copyright holder for this preprint (which was not certified by peer review) is the author/funder, who has granted bioRxiv a license to display the preprint in perpetuity. It is made available under aCC-BY 4.0 International license.

Statistical comparisons of length and radius between human and rat kidneys[5] was performed in GraphPad Prism (version: 2021), and all graphs and plots were created with Origin 2021b. For statistical comparison of normalised vessel radius and length , a p value of less than 0.05 was considered statistically significant. Log of radius and length were plotted against Strahler generation for each of the human and rat datasets, enabling a linear least squares regression. A sum of squares F test was performed with the null hypothesis that a single set of global parameters for slope and intercept would fit vessel radius or vessel length for both the rat and human cases. In the case of vessel radius $p < 0.0001$; F (DFn, DFd) = 700.6 (2, 12). In the case of vessel length $p = 0.4213$; F (DFn, DFd) = 0.9299 (2, 12).

RESULTS

HiP-CT maps the entire blood vascular network in the intact human kidney

Using HiP-CT[12,14] (**Fig. 1A**), we imaged the intact kidney of a 63-year-old male organ donor at 25 μm^3/voxel . After 3D reconstruction and pre-processing, we segmented all visible renal arteries/arterioles thus extracting the entire arterial network of the organ (**Fig. 1B**). By generating 3D renderings of the arterial network, we identified a segmental pattern of anterior, posterior, superior and inferior territories supplying the renal parenchyma (**Supplementary Video 1**). Each vascular territory (shown in different colours in **Fig. 1C**) had a corresponding renal arterial branch originating from the hilum which bifurcated before hierarchical branching towards the cortical parenchyma.

The vascular dataset consisted of a spatial graph containing 5730 end or branching points, 303,595 points, and 5,718 vessels.

Generational analysis of the network was applied to classify the vessels into established biological hierarchies. We resolved 24 topological generations, or eight Strahler generations, with an exponentially increasing branching ratio down to the eight generations (**Fig. 1F**). We mapped each generation to established anatomical groups: Strahler generations 7-8 (n = 17

bioRxiv preprint doi: https://doi.org/10.1101/2023.03.28.534566; this version posted March 29, 2023. The copyright holder for this preprint (which was not certified by peer review) is the author/funder, who has granted bioRxiv a license to display the preprint in perpetuity. It is made available under aCC-BY 4.0 International license.

vessels; mean radius = 1249 ± 797 µm) mapped to the branches of the renal artery entering the kidney hilum. Generations 5-6 comprise interlobar arteries (*n = 160* vessels; mean radius = 320 ± 131 µm), and generations 2-4 arcuate arteries (*n* = 2672 vessels; mean radius = 90 ± 52 µm). Interlobular arteries fall within generations 1-3 (*n* = 5185 vessels; mean radius = 59 ± 27µm).

The human kidney appeared to have a, lower number of generations than previously found in rat[5] (8 in human as compared to 11 in rat). To understand this discrepancy, we examined selected areas of the human kidney at higher resolution. We segmented arterioles from selected regions of interest within the same human kidney scanned at 2.6 μm^3/voxel. From these high-resolution images, we were able to segment a further three generations, corresponding to efferent and afferent arterioles as evidenced by the presence of glomeruli terminal ends of the arteriolar network **(Fig.1G)**. Thus, we are able to verify that HiP-CT of the whole human kidney can resolve the renal arterial network down to the level of interlobular arteries, and use HiP-CTs higher local resolution, to verify that the number of branching generations in the human kidney matches that of the rat.[5]

Analysis of vascular network metrics in the human kidney reveals concordance with a rodent model organism

Vascular network metrics provide a means for quantitative comparison between individuals, species or pathologies[16,17] and are increasingly used for the simulation of oxygenation, drug delivery, or generating realistic vascular networks for in silico medical trials.[18,19] These applications require metrics including branching angle, radius, tortuosity and length as inputs, and often assume adherence to e.g. Murray's Law. To our knowledge, no such metrics exists for the human kidney, and thus we report them here (**Fig. S1B-E, Table 1**).

Previously, computational models of mammalian renal blood flow have been derived from quantitative analysis of micro-CT images of the intact rat kidney vasculature[20–22] until now, it is not been possible to assess how these analyses compare to the human organ. We therefore compared our human kidney HiP-CT data with those derived from micro-CT data

bioRxiv preprint doi: https://doi.org/10.1101/2023.03.28.534566; this version posted March 29, 2023. The copyright holder for this preprint (which was not certified by peer review) is the author/funder, who has granted bioRxiv a license to display the preprint in perpetuity. It is made available under aCC-BY 4.0 International license.

of rat,[5] relating normalised vessel metrics from each species at corresponding generations of the renal arterial network. The increasing trend in vessel radius with generation from interlobular arteries to major renal artery branches was similar between human and rat kidney (**Fig. 2B**), albeit there was a significantly lower normalised vessel radius at each generation in humans as compared to rat ($p < 0.0001$).[5] Conversely, normalised vessel lengths were similar between human and rat kidney at each generation (**Fig. 2C,** $p = 0.4213$).

Branching ratio provides an indication of network symmetry, with a perfectly symmetrical network having a branching ratio of 2. It is hypothesised that the symmetry or asymmetry of a blood vascular network is indicative of constraints imparted upon its architecture by metabolic demands.[23,24]

We found that the branching ratio of the human arterial network was 2.41 whilst the rat kidney is reported as 2.85, [5] indicating that both human and rat kidney possess slight branching asymmetry as do many other mammalian networks e.g. the rat lung (3.31) and human torso. [5,24]

Murray's law which prescribes the vessel diameter ratio for parent and child vessels that minimises resistance to blood flow, is an often used constraint in branching structure growth simulations.[25] We demonstrate agreement with Murray's Law (**Fig.2D,** $r = 0.95$, $R^2 = 0.758$) for the human arterial renal network, as has previously been demonstrated for the rat.[5] In summary, branching metrics and trends are conserved between the rodent and human kidney. However, certain metrics such as vessel radius vary; an important consideration when extrapolating or translating vascular analyses from rodent to human.

Regional heterogeneity in vascular branching metrics provides a basis for local hypoxia within the kidney microenvironment

Regional heterogeneity within the kidney creates local microenvironments that enable specialised renal functions. The renal medulla possesses low oxygen tension, generating hypoxia that is inherent to the medulla's urinary concentration mechanisms. A longstanding

bioRxiv preprint doi: https://doi.org/10.1101/2023.03.28.534566; this version posted March 29, 2023. The copyright holder for this preprint (which was not certified by peer review) is the author/funder, who has granted bioRxiv a license to display the preprint in perpetuity. It is made available under aCC-BY 4.0 International license.

hypothesis, supported by MRI studies,[26] is that vascular rarefaction in acute and chronic kidney diseases results in hypoxia within the renal cortex, stimulating neighbouring cells into a pro-fibrotic phenotype and manifesting in loss of organ function.[2] Mapping the regional anatomical layout of the vasculature is fundamental to understand local microenvironments, including the generation of physiological, or susceptibility to pathological hypoxia.

To assess regional vascular heterogeneity in the human kidney, HiP-CT scans were semi-automatically segmented into hilar, medullary and cortical zones (**Fig. 3A**). The volume of each zone in addition to the number of vessels, length, radius and volume of segmented vessels within each zone were quantified (**Table 2**). Despite the majority of the volume of the human kidney being occupied by the cortex (64.7%) as compared with the medulla (27.3%) or hilum (8.0%), the cortex had the lowest vessel volume (9.5% *vs.* 14.3% *vs.* 42.8%). (NB total percentage does not sum to 100%, as vessels that straddle two regions are excluded). As a proxy for renal tissue oxygenation, we quantified (**Fig. 3B-C**) and mapped (**Fig. 3D-E**) the inter-vessel distance, reflecting the extravascular distance across which oxygen and solutes diffuse, compartmentalised by hilum, medulla, and cortex. Mean inter-vessel distances for medulla, cortex and hilum **(Table. 2)** show that the cortex has the lowest inter-vessel distance (1.3 x 103 ± 824 µm) followed by the hilum (1.5 x 103 ± 1400 µm) and medulla (1.6 x 10^3 ± 1000 µm), thus following anticipated distributions. Notably, there were large portions within the medulla where inter-vessel distance was > 4.5 mm **(Fig. 3D)**, in line with the hypoxic character of the medulla. Whilst the cortex has the lowest inter-vessel distance, small areas with high inter-vessel distance > 4.5mm were found, predominantly towards the renal capsule, which we attribute to the previously discussed resolution limit of these data (see Fig. 1G).

DISCUSSION

bioRxiv preprint doi: https://doi.org/10.1101/2023.03.28.534566; this version posted March 29, 2023. The copyright holder for this preprint (which was not certified by peer review) is the author/funder, who has granted bioRxiv a license to display the preprint in perpetuity. It is made available under aCC-BY 4.0 International license.

Owing to the limited volume of tissue imageable using modalities such as micro-CT and LSM, and comparatively low resolution of routine clinical imaging, it has been impossible, until now, to capture the entire vascular network of the intact human kidney. We have overcome these limitations using HiP-CT, enabling 3D imaging and segmentation of an entire human kidney arterial network at twenty-fold greater resolution than conventional clinical CT scanners (200 µm voxels), instead comparable to that of light microscopy (1-8 µm pixels) yet at a scale several orders of magnitude larger than that of a renal punch biopsy. The balance between imaging volume and resolution afforded by HiP-CT thus bridges the scale between local cellular structures and global tissue changes, providing quantitative vascular metrics from an intact human organ for the first time.

The metric we report here are the first of their kind and thus represent a baseline for the morphology of the human renal arterial network. As further studies are performed, our data will provide a benchmark for natural the variation in human anatomy and also for pathological variations from e.g. diabetes or renal cancer.

Using HiP-CT, we show that the human kidney's arterial network is exquisitely organised across the organ, with branching metrics optimally arranged to minimise resistance to flow akin to rodent species, whilst also possessing regional heterogeneity likely contributing to physiological gradients in local oxygen tension and susceptibility to hypoxia. Beyond biophysical modelling and providing a platform to study renal pathologies, the dataset generated has immediate practical applications, such as providing inputs for bioprinting of artificial kidneys[27] or planning tumour resection whilst preserving renal function.[28]

Limitations of this work include the low throughput of the pipeline, the resolution limit of the organ-wide scan, and the limited access to the technique, currently. Emerging solutions to these limitations are provided by, i) machine learning methods for automated segmentation of vessels from imaging data,[29,30] ii) improvements of the ESRF beamline which are already extending the resolution limit for whole organs down to 8 µm; iii) the release of the data through the Human Organ Atlas portal (https://human-organ-

bioRxiv preprint doi: https://doi.org/10.1101/2023.03.28.534566; this version posted March 29, 2023. The copyright holder for this preprint (which was not certified by peer review) is the author/funder, who has granted bioRxiv a license to display the preprint in perpetuity. It is made available under aCC-BY 4.0 International license.

atlas.esrf.eu/). Ultimately, we envisage that mapping microstructural detail will become possible at the scale of the whole kidney, providing a means to link cellular events with organ physiology and pathology.

bioRxiv preprint doi: https://doi.org/10.1101/2023.03.28.534566; this version posted March 29, 2023. The copyright holder for this preprint (which was not certified by peer review) is the author/funder, who has granted bioRxiv a license to display the preprint in perpetuity. It is made available under aCC-BY 4.0 International license.

DISCLOSURE

JJ reports fees from Boehringer Ingelheim, Roche, NHSX, Takeda and GlaxoSmithKline unrelated to the submitted work. JJ was supported by Wellcome Trust Clinical Research Career Development Fellowship 209553/Z/17/Z and the NIHR Biomedical Research Centre at University College London.

ACKNOWLEDGEMENTS

The authors would like to express their gratitude for the financial support provided by the Chan Zuckerberg Initiative DAF (2020-225394), an advised fund of SVCF, the MRC (MR/R025673/1), and ESRF beamtimes (md1252 & md1290). P.D.L. is supported by a Royal Academy of Engineering Chair in Emerging Technologies (CiET1819/10). D.J.J. is supported by a Foulkes Foundation Postdoctoral Fellowship. D.A.L. is supported by a Wellcome Trust Investigator Award (220895/Z/20/Z) and by the National Institute for Health Research (NIHR) Biomedical Research Centre at Great Ormond Street Hospital for Children NHS Foundation Trust and University College London. This research was funded in part by the Wellcome Trust [209553/Z/17/Z]. M.A. is supported by the National Institutes of Health (NIH) (HL94567 and HL134229). JJ, was also supported by the NIHR UCLH Biomedical Research Centre, UK.

AUTHOR CONTRIBUTIONS

P.D.L, R.J.S., and P.T. and C.L.W. conceptualized the project and designed experiments; P.T. designed and built instrumentation and performed HiP-CT imaging; S.R. and C.L.W. designed, managed and performed image analysis; S.R. and C.L.W. modelled, quantified and provided results; S.R., C.L.W., R.J.S., D.A.L., D.J.J., and P.D.L provided results interpretation and discussion; D.J.J. and D.A.L. provided specialist renal input; S.R., C.L.W., D. J. J., and D.A.L. wrote the paper; All authors assisted in reviewing and revising the manuscript.

bioRxiv preprint doi: https://doi.org/10.1101/2023.03.28.534566; this version posted March 29, 2023. The copyright holder for this preprint (which was not certified by peer review) is the author/funder, who has granted bioRxiv a license to display the preprint in perpetuity. It is made available under aCC-BY 4.0 International license.

DATA SHARING STATEMENT

The raw image data will be made freely available via the Human Organ Atlas (https://human-organ-atlas.esrf.eu), upon publication. Furthermore, the binary labels, spatial graph data of the arterial network of the kidney, along with the computed morphological parameters and codes, are available via the following link:

[https://zenodo.org/record/7708966#.ZBxhDnbP0uU]

REFERENCES

1. Dumas SJ, Meta E, Borri M, Luo Y, Li X, Rabelink TJ, et al.: Phenotypic diversity and metabolic specialization of renal endothelial cells. *Nat. Rev. Nephrol.* 17: 441–464, 2021
2. Long DA, Norman JT, Fine LG: Restoring the renal microvasculature to treat chronic kidney disease. *Nat. Rev. Nephrol.* 8: 244–250, 2012
3. Marsh DJ, Postnov DD, Rowland DJ, Wexler AS, Sosnovtseva O V, Holstein-Rathlou N-H: Architecture of the rat nephron-arterial network: analysis with micro-computed tomography. *Am. J. Physiol. Physiol.* 313: F351–F360, 2017
4. Perrien DS, Saleh MA, Takahashi K, Madhur MS, Harrison DG, Harris RC, et al.: Novel methods for microCT-based analyses of vasculature in the renal cortex reveal a loss of perfusable arterioles and glomeruli in eNOS-/-mice. *BMC Nephrol.* 17: 1–10, 2016
5. Nordsletten DA, Blackett S, Bentley MD, Ritman EL, Smith NP: Structural morphology of renal vasculature. *Am. J. Physiol. Circ. Physiol.* 291: H296–H309, 2006
6. Parvin N, Charlton JR, Baldelomar EJ, Derakhshan JJ, Bennett KM: Mapping vascular and glomerular pathology in a rabbit model of neonatal acute kidney injury using MRI. *Anat. Rec.* 303: 2716–2728, 2020
7. Foiret J, Zhang H, Ilovitsh T, Mahakian L, Tam S, Ferrara KW: Ultrasound localization microscopy to image and assess microvasculature in a rat kidney. *Sci. Rep.* 7: 13662, 2017
8. Huang J, Brenna C, Khan A ul M, Daniele C, Rudolf R, Heuveline V, et al.: A cationic near infrared fluorescent agent and ethyl-cinnamate tissue clearing protocol for vascular staining and imaging. *Sci. Rep.* 9: 521, 2019
9. Klingberg A, Hasenberg A, Ludwig-Portugall I, Medyukhina A, Männ L, Brenzel A, et al.: Fully automated evaluation of total glomerular number and capillary tuft size in nephritic kidneys using lightsheet microscopy. *J. Am. Soc. Nephrol.* 28: 452–459, 2017
10. Ogunlade O, Connell JJ, Huang JL, Zhang E, Lythgoe MF, Long DA, et al.: In vivo three-dimensional photoacoustic imaging of the renal vasculature in

bioRxiv preprint doi: https://doi.org/10.1101/2023.03.28.534566; this version posted March 29, 2023. The copyright holder for this preprint (which was not certified by peer review) is the author/funder, who has granted bioRxiv a license to display the preprint in perpetuity. It is made available under aCC-BY 4.0 International license.

preclinical rodent models. *Am. J. Physiol. Physiol.* 314: F1145–F1153, 2018

11. Zhao S, Todorov MI, Cai R, Rami A-M, Steinke H, Kemter E, et al.: Cellular and molecular probing of intact human organs. *Cell* 180: 796–812, 2020
12. Walsh CL, Tafforeau P, Wagner WL, Jafree DJ, Bellier A, Werlein C, et al.: Imaging intact human organs with local resolution of cellular structures using hierarchical phase-contrast tomography. *Nat. Methods* 18: 1532–1541, 2021
13. Brunet J, Walsh CL, Wagner WL, Bellier A, Werlein C, Marussi S, et al.: Preparation of large biological samples for high-resolution, hierarchical, synchrotron phase-contrast tomography with multimodal imaging compatibility. *Nat. Protoc.* 1–27, 2023
14. Brunet J, Walsh CL, Wagner WL, Bellier A, Werlein C, Marussi S, et al.: Preparation of large biological samples for high-resolution, hierarchical, multi-modal imaging. *bioRxiv* 2022
15. Mirone A, Brun E, Gouillart E, Tafforeau P, Kieffer J: The PyHST2 hybrid distributed code for high speed tomographic reconstruction with iterative reconstruction and a priori knowledge capabilities. *Nucl. Instruments Methods Phys. Res. Sect. B Beam Interact. with Mater. Atoms* 324: 41–48, 2014
16. O'Connor C, Brady E, Zheng Y, Moore E, Stevens KR: Engineering the multiscale complexity of vascular networks. *Nat. Rev. Mater.* 7: 702–716, 2022
17. Ehling J, Bábíčková J, Gremse F, Klinkhammer BM, Baetke S, Knuechel R, et al.: Quantitative micro-computed tomography imaging of vascular dysfunction in progressive kidney diseases. *J. Am. Soc. Nephrol.* 27: 520–532, 2016
18. d'Esposito A, Sweeney PW, Ali M, Saleh M, Ramasawmy R, Roberts TA, et al.: Computational fluid dynamics with imaging of cleared tissue and of in vivo perfusion predicts drug uptake and treatment responses in tumours. *Nat. Biomed. Eng.* 2: 773–787, 2018
19. Cury LFM, Maso Talou GD, Younes-Ibrahim M, Blanco PJ: Parallel generation of extensive vascular networks with application to an archetypal human kidney model. *R. Soc. Open Sci.* 8: 210973, 2021
20. Postnov DD, Marsh DJ, Postnov DE, Braunstein TH, Holstein-Rathlou N-H, Martens EA, et al.: Modeling of kidney hemodynamics: probability-based topology of an arterial network. *PLoS Comput. Biol.* 12: e1004922, 2016
21. Gardiner BS, Smith DW, O'Connor PM, Evans RG: A mathematical model of diffusional shunting of oxygen from arteries to veins in the kidney. *Am. J. Physiol. Physiol.* 300: F1339–F1352, 2011
22. Deng W, Tsubota K: Numerical Modeling and Simulation of Blood Flow in a Rat Kidney: Coupling of the Myogenic Response and the Vascular Structure. *Processes* 10: 1005, 2022
23. Brummer AB, Lymperopoulos P, Shen J, Tekin E, Bentley LP, Buzzard V, et al.: Branching principles of animal and plant networks identified by combining extensive data, machine learning and modelling. *J. R. Soc. Interface* 18: 20200624, 2021
24. Tekin E, Hunt D, Newberry MG, Savage VM: Do vascular networks branch optimally or randomly across spatial scales? *PLoS Comput. Biol.* 12: e1005223, 2016
25. Deng W, Tsubota K: Numerical simulation of the vascular structure dependence of blood flow in the kidney. *Med. Eng. Phys.* 104: 103809, 2022
26. Pruijm M, Mendichovszky IA, Liss P, Van der Niepen P, Textor SC, Lerman LO, et al.: Renal blood oxygenation level-dependent magnetic resonance imaging to measure renal tissue oxygenation: a statement paper and

bioRxiv preprint doi: https://doi.org/10.1101/2023.03.28.534566; this version posted March 29, 2023. The copyright holder for this preprint (which was not certified by peer review) is the author/funder, who has granted bioRxiv a license to display the preprint in perpetuity. It is made available under aCC-BY 4.0 International license.

systematic review. *Nephrol. Dial. Transplant.* 33: ii22–ii28, 2018

27. Lebedenko CG, Banerjee IA: Enhancing Kidney vasculature in tissue engineering—Current trends and approaches: A Review. *Biomimetics* 6: 40, 2021
28. Hsieh JJ, Purdue MP, Signoretti S, Swanton C, Albiges L, Schmidinger M, et al.: Renal cell carcinoma. *Nat. Rev. Dis. Prim.* 3: 1–19, 2017
29. Kirst C, Skriabine S, Vieites-Prado A, Topilko T, Bertin P, Gerschenfeld G, et al.: Mapping the fine-scale organization and plasticity of the brain vasculature. *Cell* 180: 780–795, 2020
30. Todorov MI, Paetzold JC, Schoppe O, Tetteh G, Shit S, Efremov V, et al.: Machine learning analysis of whole mouse brain vasculature. *Nat. Methods* 17: 442–449, 2020

bioRxiv preprint doi: https://doi.org/10.1101/2023.03.28.534566; this version posted March 29, 2023. The copyright holder for this preprint (which was not certified by peer review) is the author/funder, who has granted bioRxiv a license to display the preprint in perpetuity. It is made available under aCC-BY 4.0 International license.

Tables

Table 1. Human kidney vascular branching metrics by Strahler generation

Generation order	Number of vessels	Radius [µm]	Length [µm]
1	2869	45.7 ± 4.6	4775.9 ± 2116.1
2	1440	61.0 ± 17.7	2312 ± 1961.9
3	876	101.5 ± 38.9	2377.7 ± 2172.9
4	356	181.5 ± 58.5	3159.2 ± 2456.1
5	111	285.5 ± 91.4	4655.6 ± 3808.3
6	49	397.8 ± 170.4	5802.7 ± 3882.1
7	16	1195.6 ± 789.5	7638.8 ± 6072.1
8	1	2124	12792.8

Table 2. Human kidney vascular branching metrics by zone

	Cortex	Medulla	Hilum	Organ
Volume of tissue / µm3	8.85×10^{13} 64.7%	3.37×10^{13} 27.3%	1.09×10^{13} 8.0%	1.37×10^{14} 100.0%
Number of vessels (Vessels that belong to and cross over two regions were not included in this analysis.)	2758 48%	881 15.4%	115 2.0%	5719 100.0%
Total vessel length / µm ± STD	9.40×10^{8}	1.95×10^{6}	6.28×10^{5}	2.12×10^{7}
Mean vessel radius / µm ± STD	51.5 ± 22	115.0 ± 61	350.0 ± 184	76.0 ± 68
Mean inter-vessel distances / µm ± STD	1.3×10^{3} ± 824	1.6×10^{3} ± 1000	1.5×10^{3} ± 1400	1.3×10^{3} ± 952

bioRxiv preprint doi: https://doi.org/10.1101/2023.03.28.534566; this version posted March 29, 2023. The copyright holder for this preprint (which was not certified by peer review) is the author/funder, who has granted bioRxiv a license to display the preprint in perpetuity. It is made available under aCC-BY 4.0 International license.

FIGURE LEGENDS

Figure 1. Processing pipeline for HiP-CT imaging and quantitative analysis of the human kidney vasculature.

(A) Setup for imaging acquisition using HiP-CT at BM05; 1) tomographic stage, 2) platform, 3) sample, 4) reference sample **(B) Image processing pipeline; 1)** a 2D reconstructed image at 25 μm^3/voxel resolution; 2) binning the image by 2, 3) applying 3D median filter to increase signal to noise ratio, 4) Image normalization using background detection correction, 5) Segmentation and thresholding, 6) Labelling the four main arterial branches **(C)** 3D rendering of the segmented vascular network of a human kidney. Each of the main four branching of the renal artery entering the kidney are colour-coded **(D)** Graphical representation of topological generations within the human kidney vasculature, where each generation (G) is defined by its distance from the main branches of the renal artery (G_1) **(E)** Graphical representations of Strahler generations within the human kidney vasculature, where each generation (G) is defined by its distance from the smallest calibre vessels detected at this resolution; the interlobular arteries (G_1) **(F)** Number of vessels and number of vessels per unit volume of the whole kidney by Strahler generation. **(G)** Segmentation of high-resolution (5.2 μm^3/voxel) HiP-CT data within a randomly selected cortical region within the human kidney. Glomeruli are visible at the distal tips of the smallest vessels detected at this resolution.

Figure 2. Quantitative comparison of vascular branching metrics in human as compared to rat kidney.

(A) Plot of normalised vessel radius *vs.* Strahler generation for the human kidney vasculature (black) as compared to rat (blue). Normalisation was performed by dividing the

bioRxiv preprint doi: https://doi.org/10.1101/2023.03.28.534566; this version posted March 29, 2023. The copyright holder for this preprint (which was not certified by peer review) is the author/funder, who has granted bioRxiv a license to display the preprint in perpetuity. It is made available under aCC-BY 4.0 International license.

vessel radii by the maximum radius squared in the network. Compared to rats, the normalised vessel radius was much lower in humans at each generation ($p < 0.0001$) **(B)** Plot of normalised vessel length vs. Strahler generation for the human kidney vasculature (black) as compared to rat (blue). Normalisation was performed by dividing the vessel lengths by maximum vessel length in the network. Normalised vessel lengths were similar between human and rat kidney at each generation ($p = 0.4213$) **(C)** Assessment of the adherence of the human kidney vasculature to Murray's law. Normalized parent vessel diameter cubed is plotted against the sum of the cubed normalized daughter vessels; both axes were normalized by the maximum cubed parent vessel diameter. Using linear regression, the deviation between the line of best fit was 4.5%. In **A** and **B**, each data point represents the mean value detected at each generation and error bars represent SEM.

Figure 3. Analysis of zonal heterogeneity in vascular branching metrics within the human kidney.

(A) 3D reconstruction of semi-automatically generated masks of different zones within the human kidney including cortex (blue), medulla (yellow) and hilum (purple) **(B)** Inter-vessel distances are plotted against the total number of vessel voxels for each kidney zone **(C)** Segmented vasculature from each of the three zones, colour-coded according to zone as in **A (D)** Visual heatmap of inter-vessel distance for the entire human, where red represents the largest inter-vessel distance (> 9.65 mm) and grey (0 mm) the smallest. A zoomed 2D region of interest within cortex and medulla is shown in the red boxed region. **(E)** 2D reconstruction of the HiP-CT image associated with the zoomed region of interest above in **D.**

Supplementary Figure 1: (A) Schematic picture showing blood vessel metrics measured within the human kidney. Vessel: is defined as being between a start and end point; which correspond to either a branching point leading into another vessel branch or a terminal end where no further branches were detectable. Segments: are joining points that discretise the vessel length. Branching angle (α): is defined as the angle between the two vessels, which is

bioRxiv preprint doi: https://doi.org/10.1101/2023.03.28.534566; this version posted March 29, 2023. The copyright holder for this preprint (which was not certified by peer review) is the author/funder, who has granted bioRxiv a license to display the preprint in perpetuity. It is made available under aCC-BY 4.0 International license.

measured from the branching point to the ending points of each vessel. Tortuosity (□): is defined as the shortest distance between start and end points of a vessel dividing by the vessel length **(B)** Branching angles distribution (Number of Branching points = 2836, mean = 61.6 ± 29.6°) **(C)** Tortuosity (Number of vessels = 5718, mean = 1.35 ± 0.27) **(D)** Vessel radius against Strahler generation **(E)** Vessel radius over vessel length against Strahler generation

Supplementary Video 1: Animated 3D renderings of the arterial network, showing segmental pattern of anterior, posterior, superior and inferior territories supplying the renal parenchyma

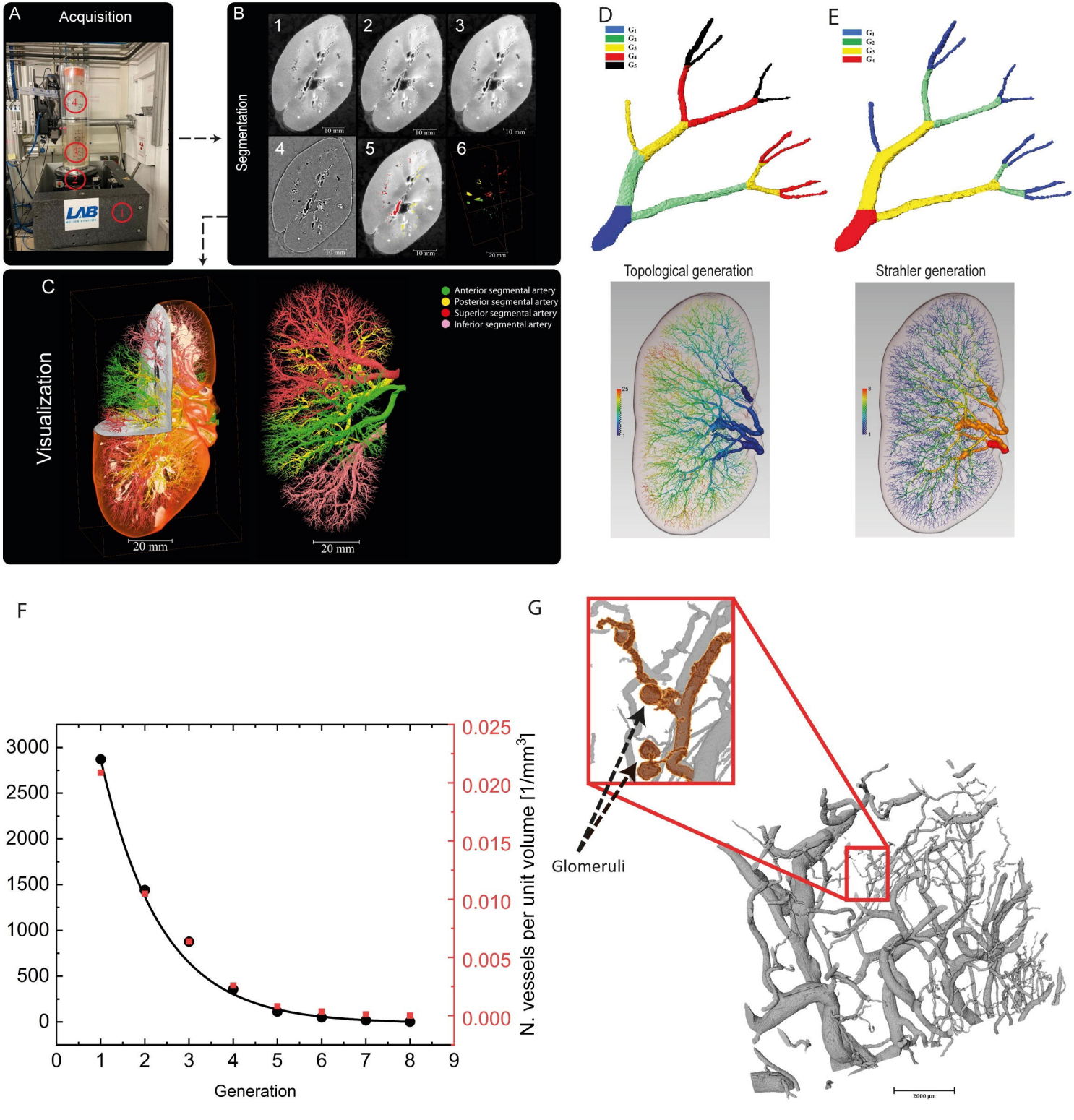
A
Acquisition
B
Segmentation
1
2
3
4
5
6
10 mm
20 mm
C
Visualization
Anterior segmental artery
Posterior segmental artery
Superior segmental artery
Inferior segmental artery
20 mm
20 mm
D
E
Topological generation
Strahler generation
F
N. vessels
N. vessels per unit volume [1/mm³]
Generation
G
Glomeruli
2000 µm

A

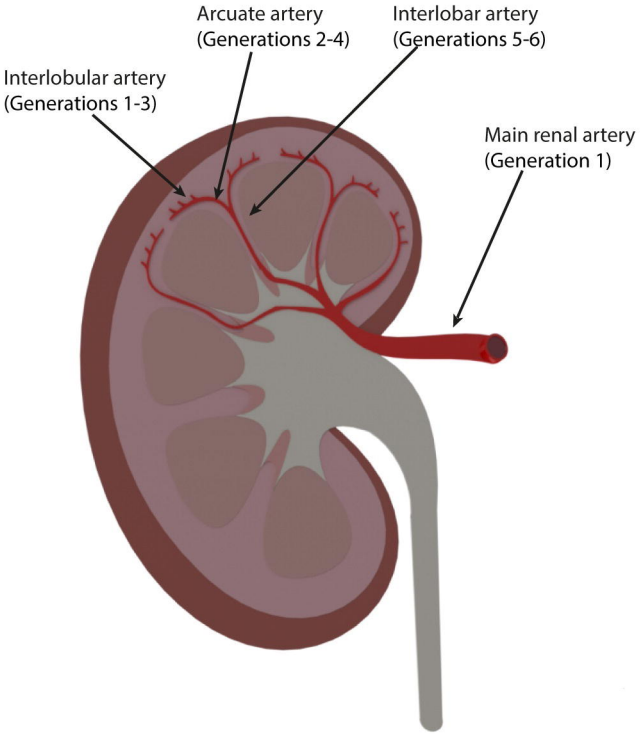
Arcuate artery
(Generations 2-4)
Interlobar artery
(Generations 5-6)
Interlobular artery
(Generations 1-3)
Main renal artery
(Generation 1)

B

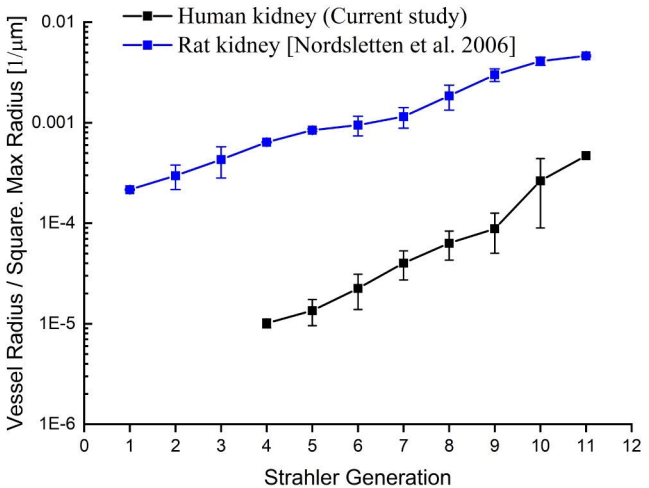
Human kidney (Current study)
Rat kidney [Nordsletten et al. 2006]
Vessel Radius / Square. Max Radius [1/µm]
0.01
0.001
1E-4
1E-5
1E-6
0 1 2 3 4 5 6 7 8 9 10 11 12
Strahler Generation

C

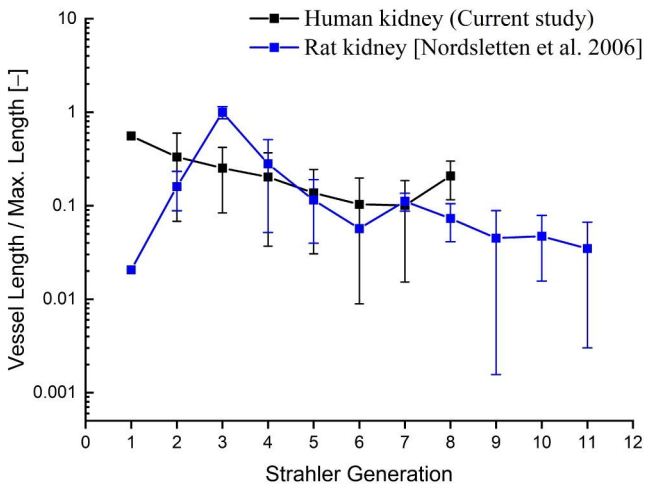
Human kidney (Current study)
Rat kidney [Nordsletten et al. 2006]
Vessel Length / Max. Length [–]
10
1
0.1
0.01
0.001
0 1 2 3 4 5 6 7 8 9 10 11 12
Strahler Generation

D

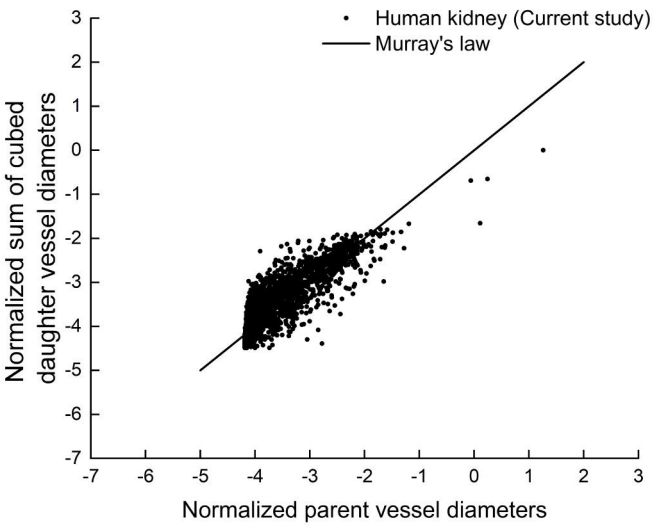
Human kidney (Current study)
Murray's law
Normalized sum of cubed daughter vessel diameters
3 2 1 0 -1 -2 -3 -4 -5 -6 -7
-7 -6 -5 -4 -3 -2 -1 0 1 2 3
Normalized parent vessel diameters

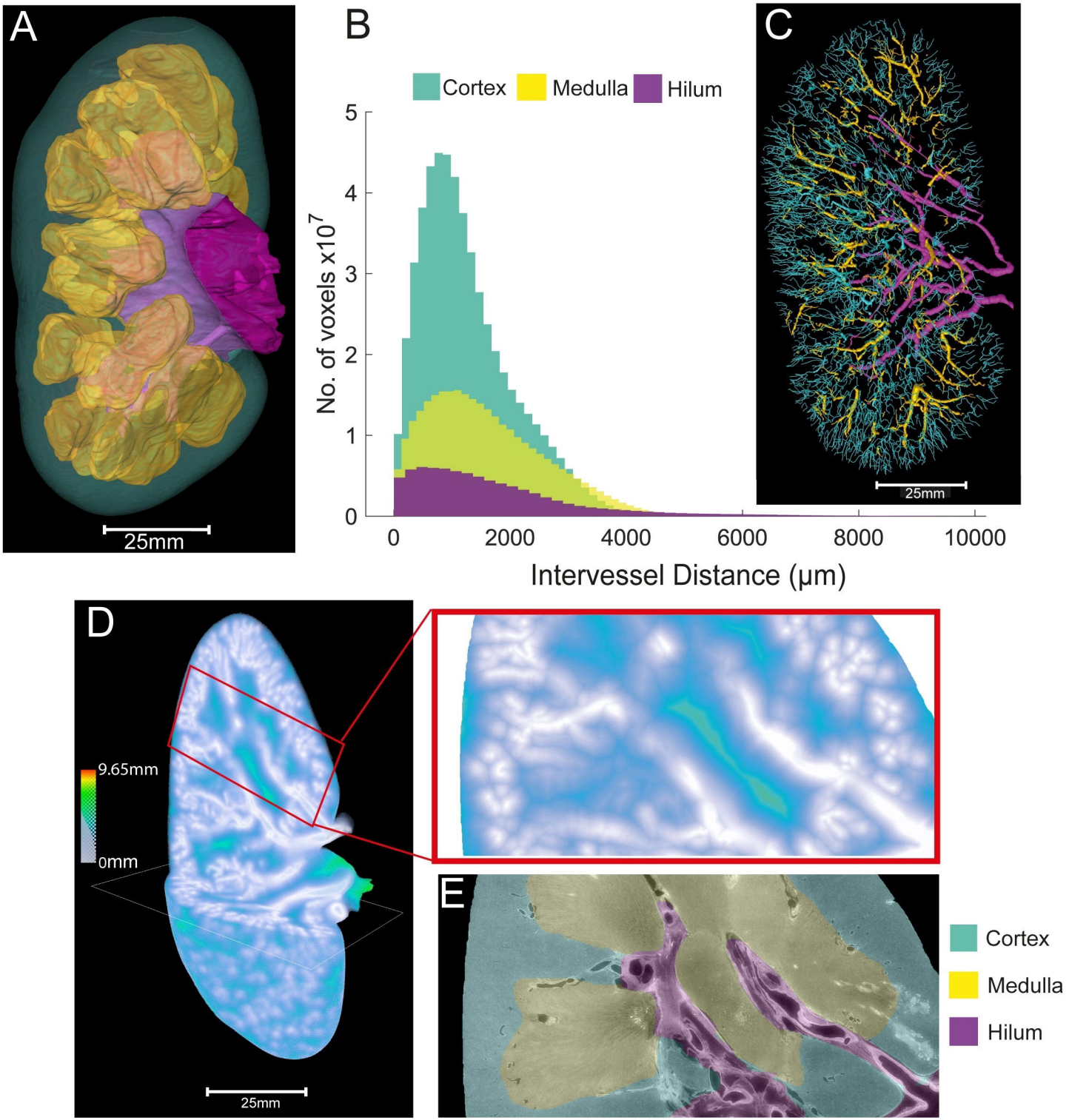
A
25mm
B
Cortex
Medulla
Hilum
No. of voxels x10^7
0
1
2
3
4
5
0
2000
4000
6000
8000
10000
Intervessel Distance (μm)
C
25mm
D
9.65mm
0mm
25mm
E
Cortex
Medulla
Hilum